Available online at www.sciencedirect.com

ScienceDirect

journal homepage: www.elsevier.com/locate/he

High power density and improved H_2 evolution reaction on MoO_3/Activated carbon composite

D.N. Sangeetha [a], R. Sowmya Holla [a], Badekai Ramachandra Bhat [b], M. Selvakumar [a,*]

[a] Department of Chemistry, Manipal Institute of Technology, Manipal Academy of Higher Education, Manipal 576104, Karnataka, India

[b] Department of Chemistry, National Institute of Technology Karnataka, Surathkal 575025 Karnataka, India

HIGHLIGHTS

- Maximum operating voltage for supercapacitor study up to 1.6 V with 1 M Na_2SO_4.
- Hybrid supercapacitor with maximum power density of 287 WKg^{-1}.
- 79% efficiency retained after 5000 charge-discharge cycles for hybrid combination.
- PDAC/h-MoO_3 catalyzed HER at much lower Tafel slope value −98 $mVdec^{-1}$.
- Faster electron transport due to PDAC defects together with hexagonal MoO_3 microrods.

GRAPHICAL ABSTRACT

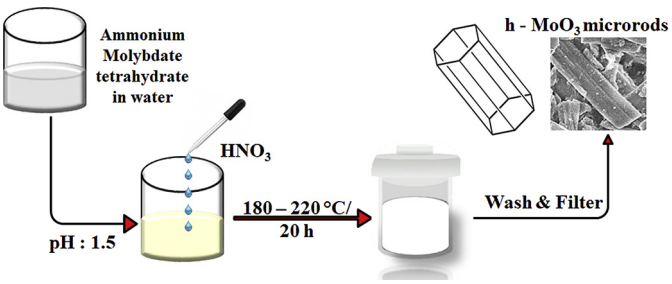

ARTICLE INFO

Article history:
Received 20 March 2019
Received in revised form
17 September 2019
Accepted 3 October 2019
Available online xxx

Keywords:
Hexagonal-MoO_3
Electrochemical impedance
Energy-density
Power-density

ABSTRACT

The formation of hexagonal MoO_3 (h- MoO_3) microrods was favoured at lower pH in the hydrothermal synthesis method. Symmetric and Hybrid supercapacitors were fabricated using h-MoO_3/plastic bottle derived activated carbon (PAC) composite in 1 M Na_2SO_4 aqueous electrolyte. The operating voltage for the aqueous electrolyte was maximized to 1.6 V with this combination. The wide operating voltage led to a maximum specific capacitance of 211 Fg^{-1}, power density of 287 W kg^{-1} and 79% efficiency even at 5000 charge-discharge cycles for the hybrid supercapacitor combination. The combined effect of PAC micropores along with the 1-D rod-shaped h-MoO_3, helped in faster charge-transfer, hence increasing the efficiency of supercapacitors. Further, the composites of defective PAC (PDAC) together with the h-MoO_3 when tested for hydrogen evolution reactions (HER), provided lesser onset potential and Tafel slope values of −0.23 mV and −93 $mVdec^{-1}$. There was a change in the structural environment of carbon due to the heteroatom doping and

* *Corresponding author*. Department of Chemistry, Manipal Institute of Technology, Manipal Academy of higher education, Manipal 576104, Karnataka, India.
E-mail address: chemselva78@gmail.com (M. Selvakumar).

https://doi.org/10.1016/j.ijhydene.2019.10.029

Tafel-slope
Overpotential

dedoping producing defects in PAC, termed as PDAC. These defects together with the hexagonal microrods of MoO_3 provided fast electron transfer towards hydrogen adsorption/desorption hence effectively producing H_2.

Introduction

Photocatalytic and electrocatalytic techniques are the two methods widely used in order to study the hydrogen evolution reaction (HER) from water splitting [1]. Among various transition metal compounds, oxides and sulphides receive a huge working attention for several applications [2,3]. HER is one such application [4–6]. The Mo family, especially MoO_3 has become the subject of increasing interest. MoO_3, a n-type layered semiconductor material attracts the researcher into several growing technological fields like supercapacitors (EC), batteries, electrochemical catalysis, chromic devices, gas/ion sensors and lubricants [7–10]. With three polymorphs, tuneable dimensions and phase, the crystalline MoO_3 makes it even more attractive towards material research. The hexagonal phase of MoO_3 (h- MoO_3), one of the phases (orthorhombic, monoclinic and hexagonal), provide a wide scope for all the above applications due to its enhanced properties than the thermodynamically stable forms. However, their synthesis is thought to be complex than the other phases [11]. Table 1 summerises the phase and morphology of MoO_3 synthesized via different techniques. Though all the three polymers have the building block, MoO_6, they differ in the type of linkage. In h-MoO_3, the MoO_6 is linked to each other by sharing the edges of the octahedral MoO_6, that is the adjacent oxygen atom link, in a zigzag fashion along the c axis.

In the context of energy-density and power-density for supercapacitor applications, redox active MoO_3 are the most suited candidates due to their reversible redox nature [12]. However, they suffer from poor electrical conductivity, short cycle stability and often disperse into the electrolyte solution during any electrochemical reaction. Hence, MoO_3 are made composites with carbon species. The high specific surface area, porous structure, stability, higher charge carrier rates of the carbon materials enhances the electrical conductivity, cycle stability, material performance of MoO_3. Also avoids material dissolution or peeling from the electrode surface. One such case is the MoO_3 nanoplate arrays grown on the carbon nanotubes (CNTs) reported by G. Saeed et al. [13]. Similar observations were recorded by B. Mendoza-Sánchez et. at., show the improved performance of MoO_3 when made composite with CNTs [14]. Further extending W. Shaheen et al., prepared a ternary composite of carbon coated MoO_3, entwined with graphene oxide stating a higher specific capacitance (SC) and admirable cycle stability for the composite than the single component electrode [15]. Graphene/NiO/MoO_3 nanosheet arrays grown on the nickel foam retained 87.9% material even after 7000 galvanostatic charge-discharge cycles [16]. Varying the weight proportions of α-MnO_2 and h-MoO_3 composites, P. M. Shahi et al. studied two different applications (EC and photocatalysis) for the composites. At a particular mass loading of h-MoO_3 (25%), they observed high ionic conductivity, better charge transferability and higher SC of 412 Fg^{-1} and 358 Fg^{-1} at 1 Ag^{-1} current density for three and two electrode systems respectively. Also obtained energy density of 50 Wh kg^{-1} with a power density of 1 kW kg^{-1} for 25% MoO_3 [17]. The application of MoO_3 composite with carbon, is not only restricted toward supercapacitors, but also extends to electrochemical reactions. S. S. J. Aravind et al. used MoO_2 dispersed over graphene that operates at a lower overpotential for hydrogen evolution [18]. HER on h-MoO_3 is not only restricted to acidic medium. It was made possible in alkaline medium with more than 40 h stability, by F. Haque et al. The strategy employed in this work was to convert the stable orthorhombic phase into hexagonal phase by doping the NH_4^+ (small) ions hydrothermally. The doping helps the exfoliation of the belt shaped MoO_3 into few sheets of h-MoO_3 having highly ordered porous structure that facilitates the diffusion of water molecules and release of HER products effectively [19]. However, the study of hydrogen evolution on MoO_3-carbon composites is limited. The present effort is hence a contribution towards this field.

Among the several synthesis techniques, hydrothermal method is the extensively used due to its ease of control over the dimensions and phases of the material by controlling the reaction parameters like solvent, temperature and time [20]. Thus, the method of pH controlled hydrothermal synthesis of h-MoO_3 was adopted in the current study. Our aim is to synthesise metastable h-MoO_3, and also to enhance its conductivity and stability by making composites with activated carbon. The composite material is then analysed as electrodes for supercapacitor and HER. This kind of composite preparation provides higher surface access for the electrolyte during charge storage of supercapacitor and also makes them operate at a lower overpotential for hydrogen evolution. The current work addresses the behaviour of h-MoO_3 microrods distributed on the activated carbon as supercapacitor and hydrogen evolution electrode material for the first time.

Materials and methods

Synthesis of h-MoO_3

h-MoO_3 was synthesized through hydrothermal technique. The synthesis procedure is as follows: to 0.1 M ammonium molybdate tetrahydrate solution, added 10 mL of 2.2 M nitric acid so as to maintain the pH of 1.5. The solution was stirred for 30 min. Loaded in an autoclave and the temperature was maintained at 180 °C for 12 h. After natural cooling, the

Please cite this article as: Sangeetha DN et al., High power density and improved H_2 evolution reaction on MoO_3/Activated carbon composite, International Journal of Hydrogen Energy, https://doi.org/10.1016/j.ijhydene.2019.10.029

Table 1 – Comparative study of synthesis method of the current work with previously reported work.

	Synthesis Method	Phase	Morphology	Ref.
α-MoO_3	Hydrothermal	Orthorhombic	Nanobelts	[3]
Carbon Fiber (CF)/MoO_3	Electrodeposition	Orthorhombic	Bamboo like pattern	[4]
MoO_3	Hydrothermal	Orthorhombic	Nanowires	[5]
MoO_3/MWCNTs	DC reactive magnetron sputtering		MoO_3 clusters on MWCNT	[6]
α-MoO_3	Sol-Gel method	Orthorhombic	Nanoplates	[7]
PANI//MoO_3	Hydrothermal method	Orthorhombic	Nanobelts	[8]
MoO_3/MWCNTs	Sonochemical Synthesis	(Amorphous nature)	Nanodots	[9]
MoO_3 in C matrix	Ball Milling	Orthorhombic	Nanoflakes	[10]
MoO_3/C sandwich	In-situ carbonization		Lamellar	[11]
α-MoO_3/MWCNT	Surfactant-assisted solvothermal method	Orthorhombic	schistose-like conglomerations	[12]
MoO_3	Exfoliation of bulk	Orthorhombic	Nanosheets	[13]
Graphene (Gr)/MoO_3	Sol-gel method followed by calcination	Orthorhombic	Nanosheets	[14]
MoO_3	Thin film deposition	Hexagonal	Microrods	[15]
α-MoO_3	Hydrothermal method	Orthorhombic	Nanobelts	[16]
α-MoO_3	Hydrothermal method	Orthorhombic	Nanorods	[17]
α-MoO_3	Layer Exfoliation	Orthorhombic	Nanosheets	[18]
α-MoO_3	Hydrothermal method followed by thin film formation via spray deposition	Orthorhombic	Nanobelts	[19]
MoO_3 in MoO_3/Polypyrrole (PPy)	Precipitation method for MoO_3 follower by Oxidative polymerization for composite synthesis	Orthorhombic	Nanobelts later converted into branch-like during composite formation	[20]
α-MoO_3	Evaporation induced self-assembly process	Orthorhombic	Porous-cubic architecture	[21]
α-MoO_3 in PPy coated α-MoO_3	Hydrothermal method	Orthorhombic	Nanobelts	[22]
MoO_3	Electrodeposition of MoO_3 on Ni	Orthorhombic	Porous films	[23]
MoO_3 in ZnO@MoO_3	Electrodeposition of MoO_3 on ZnO nanorods	Orthorhombic	Core/shell nanocables	[24]
MoO_3 in TiO_2–MoO_3	Electrodeposition of MoO_3 on TiO_2	Orthorhombic	MoO_3 shell on TiO_2 core nanowire array	[25]
MoO_3 in rGO/MoO_3/PANi	Oxidative Polymerization		Nanoparticles	[26]
MoO_3 in 3-D graphene -CNT/MoO_3	Hydrothermal method for loading MoO_3 on the 3-D graphene-CNTs	Orthorhombic	Nanoplates	[27]
1-D MoO_3	Sonochemical Dispersion method at low temperature		Nanorods	[28]
PANi-h-MoO_3	Precipitation method	hexagonal	Nanorods	[29]

(continued on next page)

Please cite this article as: Sangeetha DN et al., High power density and improved H_2 evolution reaction on MoO_3/Activated carbon composite, International Journal of Hydrogen Energy, https://doi.org/10.1016/j.ijhydene.2019.10.029

Table 1 – (continued)

	Synthesis Method	Phase	Morphology	Ref.
α-MoO_3	MoO_3 nanosheet arrays have been in-situ grown on Mo wires one-step calcination in air.	Orthorhombic	Micro cuboids	[30]
MoO_3	Microwave synthesis method	hexagonal	Nanorods	[31]
MoO_3	Hydrothermal synthesis	Hexagonal	Microrods	This work

precipitate was washed with plenty of water followed by ethanol. Dried out overnight in an air oven at 60 °C.

The brief procedure for the synthesis of PAC and PDAC is as follows. PAC is the activated carbon from plastic synthesized by carbonizing the waste plastic PET bottles and further activating with KOH activating agent. This is used in case of the EC. This PAC is not fit for any electrochemical reactions due to the inactive sites and thus were made active by insertion and removal of the nitrogen atoms in its lattice. The doping was performed hydrothermally using urea as the dopant, and the dedoping was achieved through annealing at 800 °C/N_2 atm/2 h. This is designated PDAC (defective activated carbon from plastic).

Instrumentation

The crystallographic phase of the h-MoO_3 was examined using Rigako X-Ray diffraction technique within the range of 10–80º, 5º/min scan rate, using Cu Kα_1 (1.5405) radiation. Scherrer's equation was made use for the intense peak corresponding to (210) plane, to estimate the crystallite size of h-MoO_3. The morphology and the elemental analysis were supported with ZEISS Sigma VP FE-SEM with Oxford EDS Sputtering System for SEM and tecnai 200 keV FEI for TEM. Nyquist plots were obtained from electrochemical impedance spectroscopy (EIS) within 10^3–10^5 Hz frequency range, potential of 10 mV with respect to the OCP.

Fabrication of electrodes for supercapacitor

The supercapacitor working electrode fabrication is as follows. PAC, h-MoO_3 different weight ratios (1:1, 1:2, 1:3, 2:1 and 3:1) were mixed well with acetylene black and poly (vinylidene fluoride) (80:15:5 ratios). N-methylpyrrolidone was added to the above mixture to get a slurry. The prepared slurry was then coated onto 1 cm^2 stainless steel (SS) electrode. ~5 mg/cm^2 of the electrode material loading was maintained throughout. Two PAC/h-MoO_3 electrodes separated by polypropylene regarded as Symmetric EC (SEC). While in the case of hybrid EC (HEC), PAC and PAC/h-MoO_3 was taken as the anode and cathode respectively. 1 M Na_2SO_4 electrolyte was used for the entire supercapacitor study.

Fabrication of electrodes for hydrogen evolution reaction

Glassy carbon (GC) coated with the electrocatalyst used as a working electrode for testing hydrogen evolution reaction. The material was sonicated with a mixture of water and nafion (1:5 ratio by volume) to assure proper dispersion. The ink was then drop cast onto the GC and allowed to dry. The HER was performed in three electrode set-ups with Pt and Ag/AgCl as the counter and reference electrodes. N_2 purged 0.5 M H_2SO_4 was used as the electrolyte.

Results and discussions

We notice from the SEM and FESEM images (Fig. 1a and 1c) that there is the growth of h-MoO_3 along one direction giving rod morphology. At this synthesis condition (180 °C/12 h/

Please cite this article as: Sangeetha DN et al., High power density and improved H_2 evolution reaction on MoO_3/Activated carbon composite, International Journal of Hydrogen Energy, https://doi.org/10.1016/j.ijhydene.2019.10.029

aqueous solvent), monodispersed microrods are observed. From these images (Fig. 1a and Fig. 1c) of h-MoO_3, densely dispersed microrods are observed. However, these shapes are not constant throughout. There is some irregularity in their dimensions. XRD studies helped in analysing the phase and the crystallographic structure of MoO_3 as shown in Fig. 1b. This confirms the hexagonal phase of MoO_3. Among the three polymorphs (α, β and h) of MoO_3, the hexagonal phase is metastable in nature [21,22]. No secondary impurity which correspond to any other polymorphs of MoO_3 has been detected. The strong diffraction peaks (100), (110), (200), (210), (300), (310), (320), (410), (008), (218), (430), (610) and (520) represent the hexagonal crystal phase of h-MoO_3 with reference to JCPDS-21-0569. Crystallographic size of h-MoO_3 calculated using Scherrer's equation is 17.43 nm. The MoO_6 octahedron is the basic building unit in MoO_3. Few factors like the low concentration of HNO_3, aqueous medium, short reaction time and lower reaction temperature govern the morphology and phase of MoO_3. h-MoO_3 phase formation mainly occurs due to the self-assembled MoO_6 with the assistance of the reactant precursors like NH_4^+ and H_2O. The role of these two molecules is to act as a structural directing agent promoting the growth of MoO_3 along one particular direction. In the case of h-MoO_3 it is along the c-direction, which hold higher free energy. These molecules retain the core building of h-MoO_3 during the rod formation [23]. With good accordance to the SEM results, rod-shaped microstructures are also been detected in TEM images (Fig. 1d).

The HRTEM images are shown as Fig. 2c, d and 2e, the PAC/h-MoO_3 composite formation is clearly visible in these images as marked. The rod shaped MoO_3 and the sheet morphology of PAC is clearly visible as stated in FESEM image (Fig. 2b). Form Fig. 2a it is clearly evident that the impedance behaviour of h-MoO_3 is much higher (in the order of thousands) than the activated carbon or the composite material. Such a behaviour can be attributed to the interaction of NH_4^+ ion with the H_2O molecule present in the lattice of the h-MoO_3. When an AC frequency is applied, the free movement of the ions within the h-MoO_3 is restricted. This constraint is due to the nonperiodic free energy barrier that occurs when NH_4^+ ion interacts with H_2O molecule. This barrier in turn reduces the free energy potential barrier for the free movement of ions. This further reduces the charge-transfer. Thus, a very high value is noticed for h-MoO_3 [20]. Further, in order to select the best ratios for the further fabrication of EC electrode, nyquist plots were obtained for different ratios of PAC and h-MoO_3 (1:1, 1:2, 1:3, 2:1 and 3:1). It is clearly evident that the composite possessing a straight line with a minor winding at high frequency, indicating the conducting behaviour of the electrodes. The entire Nyquist plot is divided into three sections in this case. The intercept of the AC impedance plot with the real impedance section at the higher frequency region, is the contribution of the solution resistance (R_S). Further, the electrode resistance offered for the movement of ions is the influence of charge-transfer resistance (R_{CT}). The diameter of the semicircle represents R_{CT}. The third is the linear part inclined at an angle 45° to the real axis at the region of lower frequency, the Warburg element (Z_W). However, in the case of the HEC and SEC PAC/h-MoO_3, there is distortion in this 45° inclination and it is an approximately 70° inclination in both the case. This shows

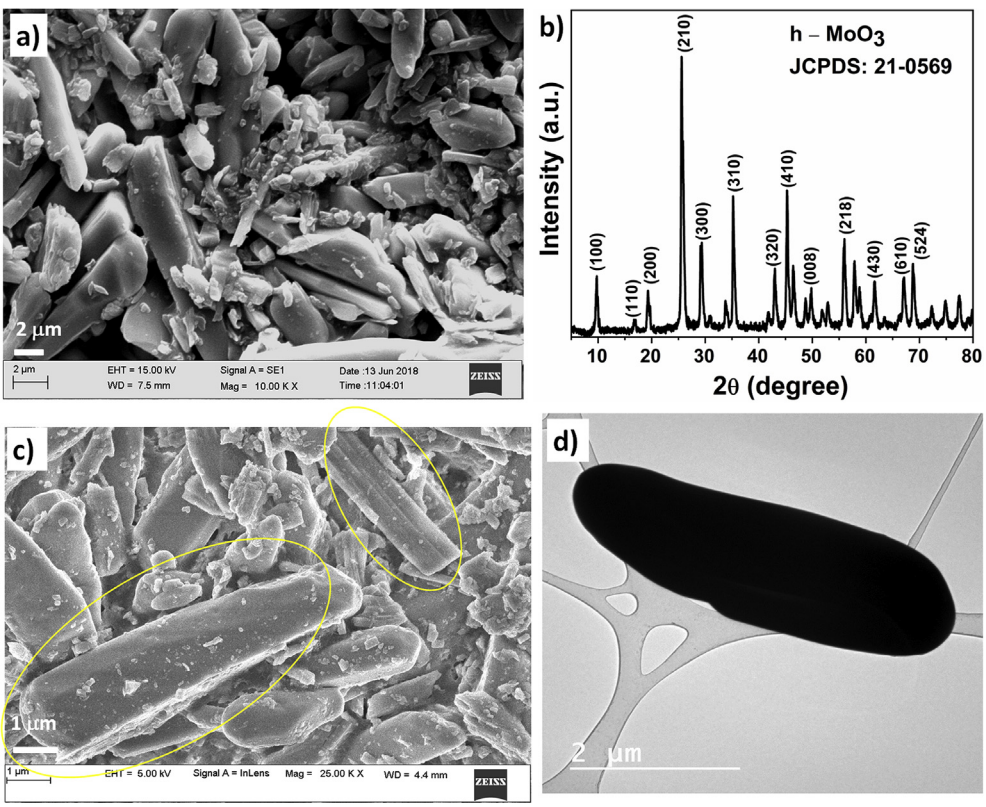

Fig. 1 – (a) SEM; (b) XRD; (c) FESEM and (d) TEM images of h-MoO_3.

Please cite this article as: Sangeetha DN et al., High power density and improved H_2 evolution reaction on MoO_3/Activated carbon composite, International Journal of Hydrogen Energy, https://doi.org/10.1016/j.ijhydene.2019.10.029

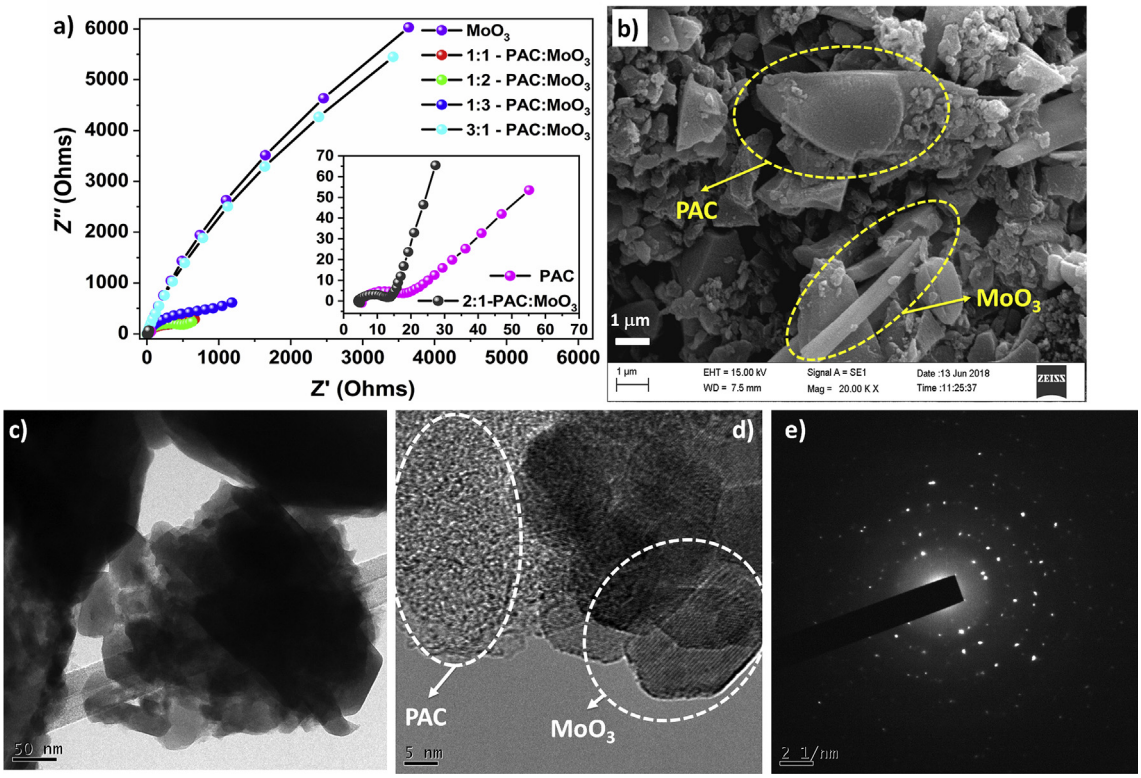

Fig. 2 – (a) Nyquist plots obtained from the EIS of PAC, different composites (1:1, 1:2, 1:3, 2:1, 3:1) of PAC; (b) FESEM; (c), (d) HR-TEM and (e) SAED of 2:1 PAC: h-MoO_3 composite.

that the PAC/h-MoO_3 in both the case (SEC and HER) is not really under the influence of the diffusion process and shows some capacitive nature. This capacitive behaviour further might be due to two particular reasons. (a) the large surface area available and (b) pseudocapacitance effect. This good behaviour is further observed in the CV even at high scan rates of 100 mVs^{-1}. Figs. 3 and 4 represents the entire set of SECs and HEC studies for PAC/h-MoO_3 composites. R_{CT} was found to be 26 Ω and Z_W 91 Ω for HEC. For SEC combination, the values for R_{CT} and Z_W were found to be 31 and 117 Ω respectively as summerised in Table 3.

In order to check the efficient behaviour of the composite, CV (at 100 mVs^{-1}) for the PAC/h-MoO_3, PAC and h-MoO_3 is recorded. As we can see in Fig. S1, the broad peak for the composite is obtained with typical rectangular behaviour. The cyclic voltammograms for SEC and HEC (Figs. 3b and 4b) is recorded at 2, 5, 10, 20, 30, 50, 80 and 100 mVs^{-1} scan rates, within 1.6 V potential range. A large potential 1.6 V is attained even in the presence of the aqueous electrolyte [24–26]. This is due to the high electrolyte concentration. A typical quasi-rectangular shape of the CV is obtained for both SEC and HEC with a wide potential range. This is distinctive to the EDLC behaviour of PAC and pseudocapacitive behaviour of h-MoO_3. Due to the pseudocapacitive MoO_3, a slight change in the quasi-rectangular behaviour is seen. As the scan rates proceeds from 2 to 100 mVs^{-1}, no much deformation in the shape of the cyclic voltammograms is noticed. Inferring good rate performance and faster charge transfer capability of PAC/h-MoO_3 composites. A maximum specific capacitance is obtained for a lower scan rate of 2 mVs^{-1}. At this scan rate, the electrolyte ions have maximum time access of both internal and external surface for charge-storage and hence the higher values. Whereas at higher scan rates, incomplete diffusion of electrolyte ions takes place and hence the decrease in the specific capacitance. The SC of SEC and HEC was calculated to be 117 and 211 Fg^{-1} at 2 mVs^{-1} respectively. The improved specific capacitance is accredited to the enhanced ionic and electronic conductivity of PAC/h-MoO_3 through dual mechanism, i.e., material with higher access of surface (due to PAC) for ion movement as well as continuous redox reactions (due to MoO_3). In a good agreement with the CV, GCD for the SEC and HEC (Figs. 3e and 4e) show a triangular symmetry and a linear slope with two regions in the discharge plot. One is a very minute IR drop followed by the discharge slope. Symmetry between charging and discharging is a visible proof of good reversibility, the behaviour of the ideal capacitor and also higher efficiency of the composite SEC and HEC. 0.5 $mAcm^{-2}$ recorded highest SC in both SEC and HEC. The SC values from discharge plot corresponding to HEC and SEC was calculated to be 159 and 114 Fg^{-1} respectively. Table 2 represent the comparison of the current work with the reported values. The electrochemical Na^+ insertion process, during charging and discharging is represented by the following equation:

$$Mo^{VI}O_3 + Na^+ + e^- \leftrightarrow Mo^{V}O_3Na \quad (1)$$

or by surface adsorption via,

$$(Mo^{VI}O_3)\ \text{surface} + Na^+ + e^- \leftrightarrow (Mo^{V}O_3Na^+)\ \text{surface} \quad (2)$$

Please cite this article as: Sangeetha DN et al., High power density and improved H_2 evolution reaction on MoO_3/Activated carbon composite, International Journal of Hydrogen Energy, https://doi.org/10.1016/j.ijhydene.2019.10.029

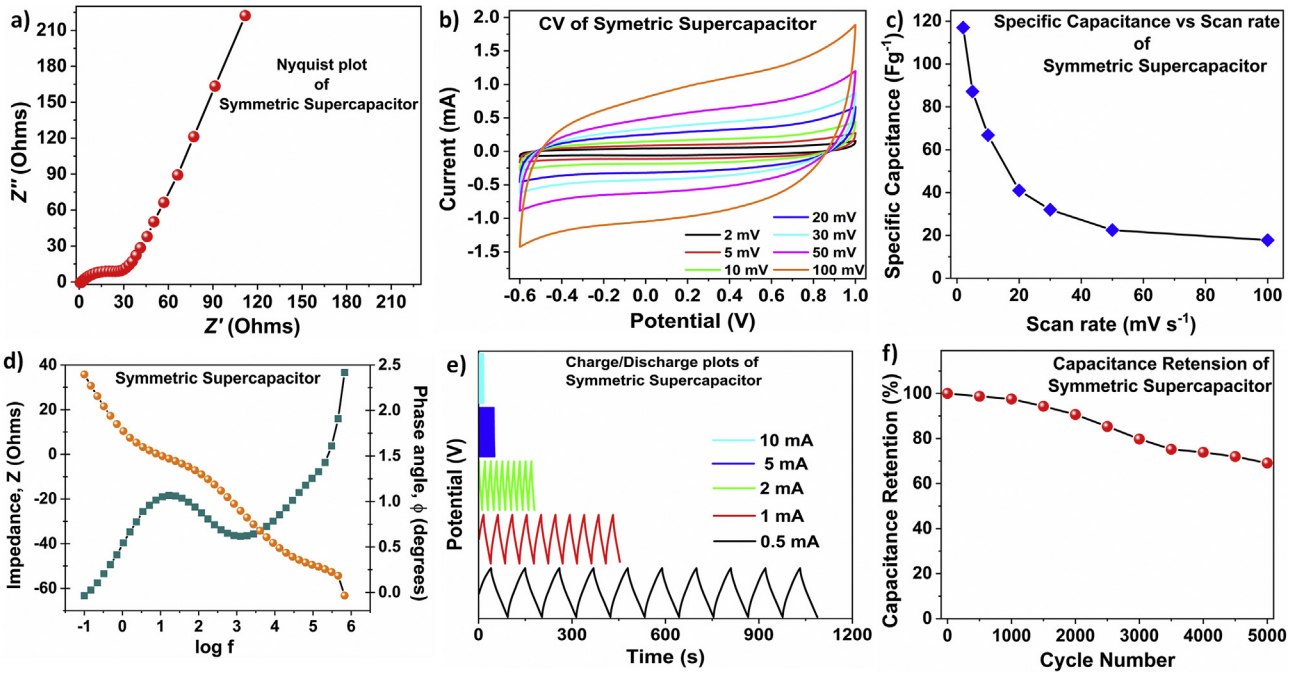

Fig. 3 – Electrochemical evaluation of 2:1 PAC/h-MoO_3 Symmetric Supercapacitor electrode (a) Nyquist plot; (b) Cyclic Voltammograms at different scan rates ranging from 2 to 100 mV s^{-1}; (c) Corresponding specific capacitance v/s scan rates; (d) time constant plot; (e) Galvanostatic charge-discharge profiles at different current densities (mA cm^{-2}) and; (f) Cycling performance at a current density of 10 mAcm^{-2} upto 5000 Cycles.

The variable oxidation states of MoO_3 as shown above, from Mo^{VI} to Mo^{V} provides an effortless ionic passage pathway to intercalate and deintercalated the Na^{+} and SO_4^{-2} electrolyte ions. On the PAC/h-MoO_3 composite electrode surface, the ease of electrons is facilitated through $Mo^{4+} \leftrightarrow Mo^{5+}$. Both the above mechanisms are sufficiently fast to yield reasonable power

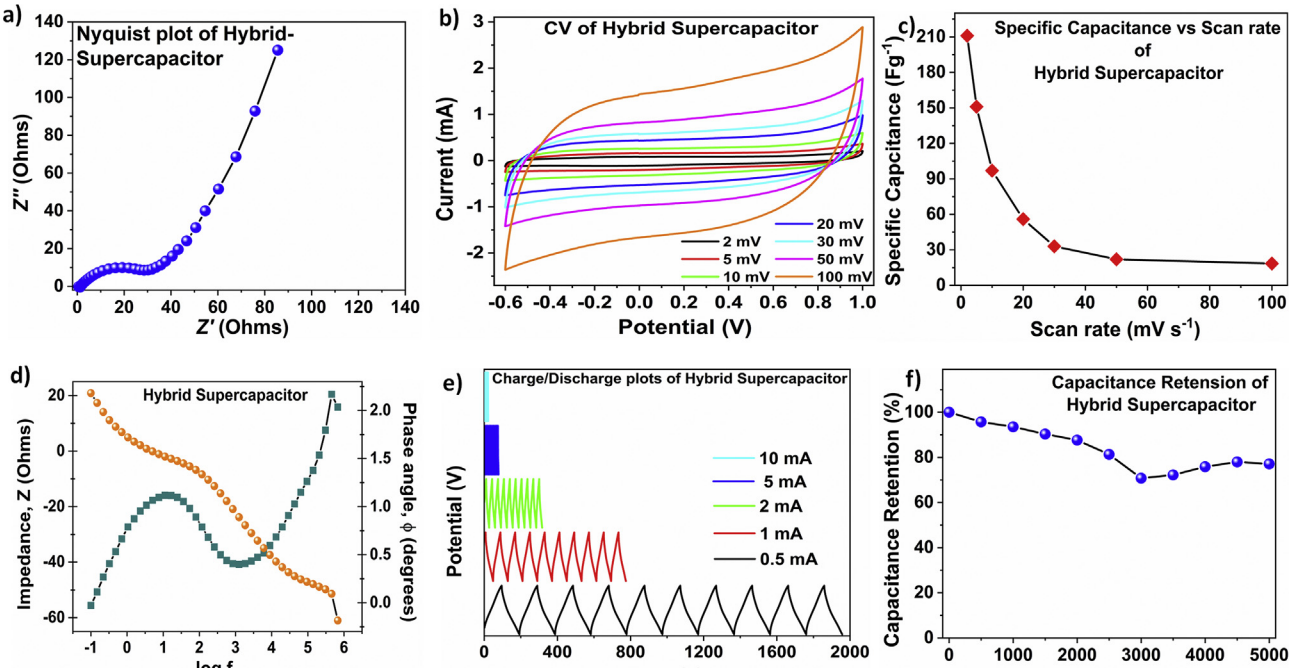

Fig. 4 – Electrochemical evaluation of Hybrid Supercapacitor electrode (a) Nyquist plot; (b) Cyclic Voltammograms at different scan rates ranging from 2 to 100 mV s^{-1}; (c) Corresponding specific capacitance v/s scan rates; (d) time constant plot; (e) Galvanostatic charge-discharge profiles at different current densities (mA cm^{-2}) and; (f) Cycling performance at a current density of 10 mAcm^{-2} upto 5000 Cycles.

Please cite this article as: Sangeetha DN et al., High power density and improved H_2 evolution reaction on MoO_3/Activated carbon composite, International Journal of Hydrogen Energy, https://doi.org/10.1016/j.ijhydene.2019.10.029

Table 2 – Comparison of operating voltage, specific capacitance, energy density, power density and cycle stability of the current work with the reported MoO_3.

Electrode Material	Electrolyte	Operating Voltage (V)	Specific Capacitance (Fg^{-1})	Energy Density ($WhKg^{-1}$)	Power Density (WKg^{-1})	Cycle Stability	Ref.
PANi@h-MoO_3 hollow nanorods	1 M H_2SO_4	0.7	247 Fg^{-1}/1 Ag^{-1}			80% after 5000 cycles	[12]
3-D graphene-CNT/MoO_3	1 M KOH	1.6	211.71 Fg^{-1}/1 Ag^{-1}	75.27	816.67	94.2% after 10000 cycles	[13]
h-MoO_3 microrod	1 M Na_2SO_4	0.7	194	7.33	1200	1000 Cycles	[31]
α-MoO_3 nanobelts	0.5 M Li_2SO_4	1.3	302 Fg^{-1}/0.1 Ag^{-1}			90% at 500 Cycles	[32]
CF/MnO_2//CF/MnO_3	1 M KOH	2.0	4.86 $mFcm^{-2}$/0.5 $mAcm^{-2}$	2.70–1.78 $\mu Whcm^{-2}$	0.53–8.30 mW cm^{-2}	89% at 500 Cycles	[33]
MoO_3-MWCNTS	1 M Na_2SO_4	2.0	210	71.6	600	90% at 2000 Cycles	[34]
MoO_3-MWCNTS	1 M Na_2SO_4	2.0	70 Fg^{-1}/10 mVs^{-1}			82% at 1000 Cycles	[35]
α-MoO_3 Nanoplates	0.5 M Li_2SO_4	0.8	280	45	450		[36]
PANI//MoO_3	1 M H_2SO_4	2.0	518 Fg^{-1}/0.5 Ag^{-1}	71.9	254	78% at 1000 Cycles	[37]
MoO_3/MWCNTs	1 M $LiClO_4$ in propylene carbonate (PC)	1.8	103	38.7	333	80% at 1000 Cycles	[38]
MoO_3 in C matrix	1 M H_2SO_4	1.0	179 Fg^{-1}/50 mA g^{-1}			80% at 1000 Cycles	[39]
MoO_3/C sandwich	1 M H_2SO_4	1.3	331 Fg^{-1}/1 Ag^{-1}	41.2	12.0 k	87.9% at 10000Cycles	[40]
Gr/MnO_2//Gr/MoO_3	1 M Na_2SO_4	2.0	307	42.6	276	1000 Cycles	[41]
α-MoO_3 nanobelts	0.5 M Li_2SO_4	0.7	369 Fg^{-1}/0.1 Ag^{-1}			95% at 500 Cycles	[42]
α-MoO_3 nanorods	1 M H_2SO_4	2.0	30 Fg^{-1}/5 mVs^{-1}	17	425	100 Cycles	[43]
MoO_3 nanosheets	1 M $LiClO_4$ in PC	2.0	540 Fg^{-1}/0.1 mVs^{-1}				[44]
α-MoO_3 nanobelts	1 M H_2SO_4	1.0	64 μFcm^{-2}			100% upto 720 Cycles	[45]
MoO_3/PPy	1 M Na_2SO_4	1.0	123 Fg^{-1}/0.27 Ag^{-1}			90% upto 200 Cycles	[46]
Porous Cubic MoO_3	1 M $LiClO_4$ in PC	2.0	150 μFcm^{-2}				[47]
Polypyrrole@α-MoO_3//AC	1 M Na_2SO_4	1.2	125 Fg^{-1}/100 mAg^{-1}	24	150		[48]
Porous MoO_3 films	1 M Na_2SO_4	1.0	50 Fg^{-1}/1.5 Ag^{-1}				[49]
ZnO@MoO_3	1 M Na_2SO_4	1.5	236 Fg^{-1}/5 mVs^{-1}			1000 Cycles	[50]
rGO/MoO_3/PANi	1 M H_2SO_4	1.2	553 Fg^{-1}	76.8–28.6	273.3–10294.3	86.6%	[51]
	1 M Na_2SO_4		363 Fg^{-1}/1 m Vs^{-1}	72.6–13.3	217.7–3993.8	73.4% after 200 cycles	
MoO_3-rGO nanocomposites	0.5 M Na_2SO_4	0.8	22.83 Fg^{-1}/0.3 Ag^{-1}				[52]
PANi/MoO_3/Graphene nanoplates	1 M H_2SO_4	1.1	593 Fg^{-1}/1 Ag^{-1} & 734 Fg^{-1}/ 1 mVs^{-1}	96.68–55.5	550.4–1679.99	92.4% after 1000 cycles	[53]
PPy@MoO_3/rGO	0.5 M K_2SO_4	1.2	175 Fg^{-1}/100 mAg^{-1}			88% after 600 cycles	[54]
PPy/MoO_3	1 M H_2SO_4	1.0	687 Fg^{-1}/1 Ag^{-1}			83% after 3000 cycles	[55]
Intertwined MoO_3-MWCNTs	1 M NaOH	1.5	178 Fg^{-1}				[56]
Hierarchical α-MoO_3 -Mo	PVA/LiCl gel electrolyte	1.5	7.68 $mFcm^{-1}$/2 mVs^{-1}	~1.04 m $Whcm^{-3}$	0.235 Wcm^{-3}	~100% even after 4000 cycles	[57]
h-MoO_3 nanorods	1 M Na_2SO_4	1.8	238 Fg^{-1}	27	225	87% after 5000 cycles	[58]
h-MoO_3 microrods	0.5 M Na_2SO_4	1.6	211 Fg^{-1}	22	287	82% after 5000 cycles	This work

Please cite this article as: Sangeetha DN et al., High power density and improved H_2 evolution reaction on MoO_3/Activated carbon composite, International Journal of Hydrogen Energy, https://doi.org/10.1016/j.ijhydene.2019.10.029

densities [27]. Thus, there is a combination of (a) adsorption/desorption of Na^+ and SO_4^{-2} ions on the PAC/h-MoO_3 surface i.e., an EDLC charge storage mechanism and (b) intercalation and deintercalation of the charged Na^+ and SO_4^{-2} ions in the pores of the PAC/h-MoO_3 composite, resulting in continuous redox reaction i.e., pseudocapacitance mechanism. 5000 charge-discharge cycles were run so as to determine the long-term stability of the SEC and HEC. 69 and 79% of the initial capacitance was retained by SEC and HEC over 5000 cycles. Table 3 includes the set of values calculated for SEC and HEC from the nyquist plot, cyclic voltammograms and charge-discharge cycles.

Electrochemical HER activity of h-MoO_3, PDAC and PDAC/h-MoO_3 were tested in 0.5 M H_2SO_4 solution. In 0.5 M H_2SO_4, used as an electrolyte, hydrogen was liberated due to the electrochemical reduction of H^+ to H_2 at the cathode ($2H_{(aq)}^+ + 2e^- \rightarrow H_{2(g)}$). The mechanism involved three steps.

Step 1. The proton adsorption with a charge transfer at the electrode surface (Volmer Step)

$$H_3O^+ + e^- + (PDAC/h-MoO_3) \leftrightarrow (PDAC/h-MoO_3)\,H_{ads} + H_2O;\ b = \frac{2.3RT}{\propto F} \approx 120 mV dec^{-1}$$

Step 2. Step 1 followed by electrochemical desorption step (Heyrovsky reaction) and involves a combination of the surface hydrogen atom with the solvated proton.

$$(PDAC/h-MoO_3)\,H_{ads} + H_3O^+ + e^- \rightarrow PDAC/h-MoO_3 + H_2 + H_2O;\ b = \frac{2.3RT}{(1+\propto)F} \approx 40 mV dec^{-1}$$

Step 3. Or through recombination step (Tafel reaction). i.e., a combination of hydrogen atoms to give a molecule of hydrogen.

$$2(PDAC/h-MoO_3)\,H_{ads} \rightarrow 2PDAC/h-MoO_3 + H_2;\quad b = \frac{2.3RT}{2F} \approx 30 mV dec^{-1}$$

b is the Tafel slope value calculated by Tafel plot fitment with the Tafel equation i.e., $\eta = a + blog\,|j|$(η represents the overpotential value, j the current density); 120, 40, 30 $mVdec^{-1}$ are the theoretical Tafel Slope values corresponding to the above mentioned steps; R represents ideal gas constant; T the absolute temperature; α the electron transfer coefficient ($\alpha = 0.5$); F the Faraday's constant. The evolution of the HER on the PDAC/MoO_3 electrode surface was determined through the values of Tafel slope. However, H_2 evolution was due to the combination of either of the steps 2 or 3 with the Volmer step. The entire HER proceeds either through Volmer-Tafel mechanism (chemical desorption of hydrogen) or through Volmer-Heyrovsky mechanism (electrochemical desorption of hydrogen) [28–30].

Table 4 – Summary of the onset potential, overpotential and Tafel slope values of the electrode materials.

Electrode	Onset Potential (mV)	Overpotential (mV)	Tafel Slope ($mVdec^{-1}$)
PAC	–	−378	−232
PAC/h-MoO_3	−0.45	−282	−169
PDAC	−0.41	−285	−176
h-MoO_3	−0.34	−212	−108
PDAC/h-MoO_3	−0.23	−203	−93

As compared to h-MoO_3 and PDAC, the composite electrode PDAC/h-MoO_3 shows good hydrogen evolution at an overpotential of the potential of 203 mV. The values are tabulated in Table 4. On observation, it is noteworthy that the integration of the electrocatalyst h-MoO_3 on the conducting substrate is remarkably important for the improvement of the whole performance. The PDAC act as a conducting substrate which leads to the enhancement of hydrogen evolution on the electrode substrate. Further, in contrast with the PDAC and h-MoO_3, as shown in Fig. 5b and c, PDAC/h-MoO_3 shows excellent electroactivity with −0.23 mV onset potential. Tafel slope is yet another parameter to understand the reaction mechanism and the electrochemical activity of the electrode. Among the three steps (Volmer, Heyrovsky and Tafel), the Volmer step determines the rate of the reaction. The value is derived from the linear part of Tafel slope under a small overpotential. The value of 93 mV per decade is obtained for PDAC/h-MoO_3 composite, which is better than h-MoO_3 and PDAC alone. The synergetic effect of the nitrogen dedoped sites of the conducting carbon with the one-dimensional rod-shaped metastable h-MoO_3 contributes to the reduced values of overpotential and onset potential in case of the PDAC/h-MoO_3 composite. The h-MoO_3 facilitates the ease of electron transport along the c-direction for faster activity. The comparative study of PAC and PDAC given in Fig. 5b, c, showed that PAC doesn't have any electrochemical hydrogen evolution at its surface as represented in LSV. It is almost a straight line parallel to x-axis. While PAC/h-MoO_3 shows hydrogen evolution at its surface. However, its performance is comparable to that of h-MoO_3. From this we could infer that the HER performance on

Table 3 – Summary of the calculated values for symmetric and hybrid PAC/h-MoO_3 EC.

Type	Specific Capacitance from CV (Fg^{-1})	Specific Capacitance from GCD (Fg^{-1})	ESR (Ω)	R_{CT} (Ω)	Z_w (Ω)	Energy Density ($WhKg^{-1}$)	Power Density (WKg^{-1})	N (%)	Time constant (ms.)
Symmetric EC	117	114	1.50	31	117	17	155	93	27
Hybrid EC	211	159	1.14	26	91	22	287	82	26

Please cite this article as: Sangeetha DN et al., High power density and improved H_2 evolution reaction on MoO_3/Activated carbon composite, International Journal of Hydrogen Energy, https://doi.org/10.1016/j.ijhydene.2019.10.029

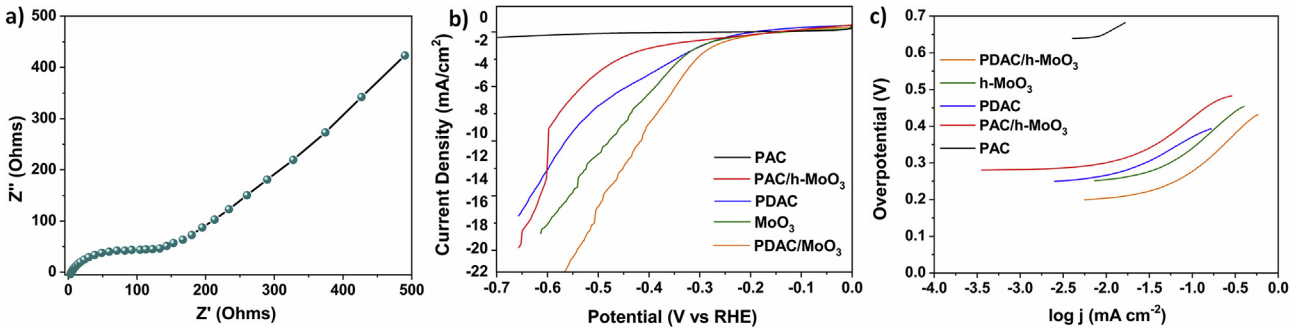

Fig. 5 – (a) Nyquist plot for of PDAC/h-MoO_3 Composite; Electrochemical HER performance of PDAC, h-MoO_3, PDAC/h-MoO_3 Composite (b) LSV and (c) Tafel plots.

PAC/h-MoO_3 is due to the h-MoO_3. PAC doesn't contribute towards hydrogen evolution performance within this potential range. The stability of the material couldn't be analysed beyond 100 CV cycles at a scan rate of 10 mVs^{-1}, as the material started peeling out from the electrode.

Conclusion

In conclusion, a low temperature, lower acidic condition and controlled pH hydrothermal synthesis technique were adopted for the synthesis of high pure-metastable hexagonal phase MoO_3. The h- MoO_3 with higher impedance value manifests no good for any practical applications. Our work demonstrates the use of carbon to improvise the electrical conductivity of the h-MoO_3. The composite material compensates the major problem of conductivity for applications like supercapacitors and hydrogen evolution. Further, the use of 1 M Na_2SO_4 facilitated a wide potential range of 1.6 V, for PAC/h-MoO_3 as supercapacitors, with 79% material retention even after 5000 working cycles. The synergetic effect of the defective activated carbon and h-MoO_3 composite show higher HER activity with lesser onset potential and small Tafel slope of 93 mV per decade, much better than h-MoO_3 or PDAC alone. This improved HER could be credited to the more active sites, improved conductivity due to the hand-in-hand functioning of the PAC and h-MoO_3 as composite material. Overall the idea of PAC/h-MoO_3 composite system for supercapacitor and hydrogen evolution provides a deeper sense in terms of activity, stability and conductivity when compared to the h-MoO_3 or PAC alone. Thus, the current concept could be an important development to study and work with the carbon-MoO_3 based composites for developing a higher performance electrode material for supercapacitors as well as to perform several real-time electrochemical applications.

Acknowledgement

The author renders heartfelt thanks for the instrumental and laboratory support offered by the Host Institute Manipal Academy of Higher Education.

Appendix A. Supplementary data

Supplementary data to this article can be found online at https://doi.org/10.1016/j.ijhydene.2019.10.029.

REFERENCES

[1] Alizadeh M, Tong GB, Mehmood MS, Qader KW, Rahman SA, Shokri B. Band engineered Al-rich InAlN thin films as a promising photoanode for hydrogen generation from solar water splitting. Sol Energy Mater Sol Cells 2018;185:445–55. https://doi.org/10.1016/j.solmat.2018.05.058.

[2] Wang Y, Ou JZ, Balendhran S, Chrimes AF, Mortazavi M, Yao DD, et al. Electrochemical control of photoluminescence in two-dimensional MoS_2 nanoflakes. ACS Nano 2013;7:10083–93. https://doi.org/10.1021/nn4041987.

[3] Wang Y, Ou JZ, Chrimes AF, Carey BJ, Daeneke T, Alsaif MMYA, et al. Plasmon resonances of highly doped two-dimensional MoS_2. Nano Lett 2015;15:883–90. https://doi.org/10.1021/nl503563g.

[4] Mascaretti L, Ferrulli S, Mazzolini P, Casari CS, Russo V, Matarrese R, et al. Hydrogen-treated hierarchical titanium oxide nanostructures for photoelectrochemical water splitting. Sol Energy Mater Sol Cells 2017;169:19–27. https://doi.org/10.1016/j.solmat.2017.04.045.

[5] Kumar DP, Kumari VD, Karthik M, Sathish M, Shankar MV. Shape dependence structural, optical and photocatalytic properties of TiO_2 nanocrystals for enhanced hydrogen production via glycerol reforming. Sol Energy Mater Sol Cells 2017;163:113–9. https://doi.org/10.1016/j.solmat.2017.01.007.

[6] Sangeetha DN, Selvakumar M. Active-defective activated carbon/MoS_2 composites for supercapacitor and hydrogen evolution reactions. Appl Surf Sci 2018;453:132–40. https://doi.org/10.1016/j.apsusc.2018.05.033.

[7] Ren G, Zhang BY, Yao Q, Zavabeti A, Huertas CS, Brkljača R, et al. An ultrasensitive silicon photonic ion sensor enabled by 2D plasmonic molybdenum oxide. Small 2019;15:1–10. https://doi.org/10.1002/smll.201805251.

[8] Zhang BY, Zavabeti A, Chrimes AF, Haque F, O'Dell LA, Khan H, et al. Degenerately hydrogen doped molybdenum oxide nanodisks for ultrasensitive plasmonic biosensing. Adv Funct Mater 2018;28:1–13. https://doi.org/10.1002/adfm.201706006.

[9] Zou J, Zeng H, Wang Y, Li Y. H+ intercalation into molybdenum oxide nanosheets under AFM tip bias. Phys Status Solidi Rapid Res Lett 2018;12:4–7. https://doi.org/10.1002/pssr.201700439.

Please cite this article as: Sangeetha DN et al., High power density and improved H_2 evolution reaction on MoO_3/Activated carbon composite, International Journal of Hydrogen Energy, https://doi.org/10.1016/j.ijhydene.2019.10.029

[10] Zheng L, Xu Y, Jin D, Xie Y. Novel metastable hexagonal MoO_3 nanobelts: synthesis, photochromic, and electrochromic properties. Chem Mater 2009;21:5681–90. https://doi.org/10.1021/cm9023887.
[11] Song J, Ni X, Gao L, Zheng H. Synthesis of metastable h-MoO_3 by simple chemical precipitation. Mater Chem Phys 2007;102:245–8. https://doi.org/10.1016/j.matchemphys.2006.12.011.
[12] Kumar V, Lee PS. Redox active polyaniline-h-MoO_3 hollow nanorods for improved pseudocapacitive performance. J Phys Chem C 2015;119:9041–9. https://doi.org/10.1021/acs.jpcc.5b00153.
[13] Saeed G, Kumar S, Kim NH, Lee JH. Fabrication of 3D graphene-CNTs/α-MoO_3 hybrid film as an advance electrode material for asymmetric supercapacitor with excellent energy density and cycling life. Chem Eng J 2018;352:268–76. https://doi.org/10.1016/j.cej.2018.07.026.
[14] Mendoza-Sánchez B, Hanlon D, Coelho J, O'Brien S, Pettersson H, Coleman J, et al. An investigation of the energy storage properties of a 2D α-MoO3-SWCNTs composite films. 2D Mater 2017;4:1–8. https://doi.org/10.1088/2053-1583/4/1/015005.
[15] Shaheen W, Warsi MF, Shahid M, Khan MA, Asghar M, Ali Z, et al. Carbon coated MoO_3 nanowires/graphene oxide ternary nanocomposite for high-performance supercapacitors. Electrochim Acta 2016;219:330–8. https://doi.org/10.1016/j.electacta.2016.09.069.
[16] Zeng W, Zhang G, Hou S, Wang T, Duan H. Facile synthesis of graphene@NiO/MoO_3 composite nanosheet arrays for high-performance supercapacitors. Electrochim Acta 2015;151:510–6. https://doi.org/10.1016/j.electacta.2014.11.088.
[17] Shafi PM, Dhanabal R, Chithambararaj A, Velmathi S, Bose AC. α-MnO_2/h-MoO_3 hybrid material for high performance supercapacitor electrode and photocatalyst. ACS Sustainable Chem Eng 2017;5:4757–70. https://doi.org/10.1021/acssuschemeng.7b00143.
[18] Aravind SSJ, Costa M, Pereira V, Mugweru A, Ramanujachary K, Vaden TD. Molybdenum/graphene - based catalyst for hydrogen evolution reaction synthesized by a rapid photothermal method. Int J Hydrogen Energy 2014;39:11528–36. https://doi.org/10.1016/j.ijhydene.2014.05.129.
[19] Haque F, Zavabeti A, Zhang BY, Datta RS, Yin Y, Yi Z, et al. Ordered intracrystalline pores in planar molybdenum oxide for enhanced alkaline hydrogen evolution. J Mater Chem A 2019;7:257–68. https://doi.org/10.1039/c8ta08330d.
[20] Chithambararaj A, Rajeswari Yogamalar N, Bose AC. Hydrothermally synthesized h-MoO_3 and α-MoO_3 nanocrystals: new findings on crystal-structure-dependent charge transport. Cryst Growth Des 2016;16:1984–95. https://doi.org/10.1021/acs.cgd.5b01571.
[21] Wang S, Dou K, Dong Y, Zou Y, Zeng H. Supercapacitor based on few-layer MoO_3 nanosheets prepared by solvothermal method. Int J Nanomanufacturing 2016;12:404. https://doi.org/10.1504/IJNM.2016.079225.
[22] Zhou L, Yang L, Yuan P, Zou J, Wu Y, Yu C. α-MoO3 nanobelts: a high performance cathode material for lithium ion batteries. J Phys Chem C 2010;114:21868–72. https://doi.org/10.1021/jp108778v.
[23] Pan W, Tian R, Jin H, Guo Y, Zhang LL, Wu X, et al. Structure, optical, and catalytic properties of novel hexagonal metastable h-MoO_3 nano- and microrods synthesized with modified liquid-phase processes. Chem Mater 2010;22:6202–8. https://doi.org/10.1021/cm102703s.
[24] Demarconnay L, Raymundo-Piñero E, Béguin F. A symmetric carbon/carbon supercapacitor operating at 1.6 v by using a neutral aqueous solution. Electrochem Commun 2010;12:1275–8. https://doi.org/10.1016/j.elecom.2010.06.036.
[25] Béguin F, Presser V, Balducci A, Frackowiak E. Carbons and electrolytes for advanced supercapacitors. Adv Mater 2014;26:2219–51. https://doi.org/10.1002/adma.201304137.
[26] Fic K, Lota G, Meller M, Frackowiak E. Novel insight into neutral medium as electrolyte for high-voltage supercapacitors. Energy Environ Sci 2012;5:5842–50. https://doi.org/10.1039/c1ee02262h.
[27] Liang R, Cao H, Qian D. MoO_3 nanowires as electrochemical pseudocapacitor materials. Chem Commun 2011;47:10305–7. https://doi.org/10.1039/c1cc14030b.
[28] Liu X, Gao S, Yang P, Wang B, Ou JZ, Liu Z, et al. Synergetic coupling of Pd nanoparticles and amorphous MoSx toward highly efficient electrocatalytic hydrogen evolution reactions. Appl Mater Today 2018;13:158–65. https://doi.org/10.1016/j.apmt.2018.09.001.
[29] Liu Z, Zhang X, Wang B, Xia M, Gao S, Liu X, et al. Amorphous MoS x -coated TiO_2 nanotube Arrays for enhanced electrocatalytic hydrogen evolution reaction. J Phys Chem C 2018;122:12589–97. https://doi.org/10.1021/acs.jpcc.8b01678.
[30] Wang Y, Carey BJ, Zhang W, Chrimes AF, Chen L, Kalantar-Zadeh K, et al. Intercalated 2D MoS_2 utilizing a simulated sun assisted process: reducing the HER overpotential. J Phys Chem C 2016;120:2447–55. https://doi.org/10.1021/acs.jpcc.5b10939.
[31] Pujari RB, Lokhande VC, Kumbhar VS, Chodankar NR, Lokhande CD. Hexagonal microrods architectured MoO3 thin film for supercapacitor application. J Mater Sci Mater Electron 2016;27:3312–7. https://doi.org/10.1007/s10854-015-4160-3.
[32] Li J, Liu X. Preparation and characterization of α-MoO_3 nanobelt and its application in supercapacitor. Mater Lett 2013;112:39–42. https://doi.org/10.1016/j.matlet.2013.08.094.
[33] Noh J, Yoon CM, Kim YK, Jang J. High performance asymmetric supercapacitor twisted from carbon fiber/MnO_2 and carbon fiber/MoO_3. Carbon N Y 2017;116:470–8. https://doi.org/10.1016/j.carbon.2017.02.033.
[34] Shakir I, Shahid M, Cherevko S, Chung CH, Kang DJ. Ultrahigh-energy and stable supercapacitors based on intertwined porous MoO_3-MWCNT nanocomposites. Electrochim Acta 2011;58:76–80. https://doi.org/10.1016/j.electacta.2011.08.076.
[35] Aravinda LS, Nagaraja KK, Bhat KU, Bhat BR. Magnetron sputtered MoO_3/carbon nanotube composite electrodes for electrochemical supercapacitor. J Electroanal Chem 2013;699:28–32. https://doi.org/10.1016/j.jelechem.2013.03.022.
[36] Tang W, Liu L, Tian S, Li L, Yue Y, Wu Y, et al. Aqueous supercapacitors of high energy density based on MoO_3 nanoplates as anode material. Chem Commun 2011;47:10058–60. https://doi.org/10.1039/c1cc13474d.
[37] Peng H, Ma G, Mu J, Sun K, Lei Z. Low-cost and high energy density asymmetric supercapacitors based on polyaniline nanotubes and MoO_3 nanobelts. J Mater Chem A 2014;2:10384–8. https://doi.org/10.1039/C4TA01899K.
[38] Mahmood Q, Yun HJ, Kim WS, Park HS. Highly uniform deposition of MoO_3 nanodots on multiwalled carbon nanotubes for improved performance of supercapacitors. J Power Sources 2013;235:187–92. https://doi.org/10.1016/j.jpowsour.2013.01.165.
[39] Tao T, Chen Q, Hu H, Chen Y. MoO3nanoparticles distributed uniformly in carbon matrix for supercapacitor applications. Mater Lett 2012;66:102–5. https://doi.org/10.1016/j.matlet.2011.08.028.
[40] Ji H, Liu X, Liu Z, Yan B, Chen L, Xie Y, et al. In situ preparation of sandwich MoO_3/C hybrid nanostructures for high-rate and ultralong-life supercapacitors. Adv Funct

Please cite this article as: Sangeetha DN et al., High power density and improved H_2 evolution reaction on MoO_3/Activated carbon composite, International Journal of Hydrogen Energy, https://doi.org/10.1016/j.ijhydene.2019.10.029

Mater 2015;25:1886–94. https://doi.org/10.1002/adfm.201404378.
[41] Chang J, Jin M, Yao F, Kim TH, Le VT, Yue H, et al. Asymmetric supercapacitors based on graphene/MnO_2 nanospheres and graphene/MoO_3 nanosheets with high energy density. Adv Funct Mater 2013;23:5074–83. https://doi.org/10.1002/adfm201301851.
[42] Jiang J, Liu J, Peng S, Qian D, Luo D, Wang Q, et al. Facile synthesis of α-MoO_3 nanobelts and their pseudocapacitive behavior in an aqueous Li_2SO_4 solution. J Mater Chem A 2013;1:2588. https://doi.org/10.1039/c2ta01120d.
[43] Shakir I, Shahid M, Yang HW, Kang DJ. Structural and electrochemical characterization of ??-MoO3 nanorod-based electrochemical energy storage devices. Electrochim Acta 2010;56:376–80. https://doi.org/10.1016/j.electacta.2010.09.028.
[44] Hanlon D, Backes C, Higgins TM, Hughes M, O'Neill A, King P, et al. Production of molybdenum trioxide nanosheets by liquid exfoliation and their application in high-performance supercapacitors. Chem Mater 2014;26:1751–63. https://doi.org/10.1021/cm500271u.
[45] Mendoza-Sánchez B, Brousse T, Ramirez-Castro C, Nicolosi V, Grant P S. An investigation of nanostructured thin film α-MoO_3 based supercapacitor electrodes in an aqueous electrolyte. Electrochim Acta 2013;91:253–60. https://doi.org/10.1016/j.electacta.2012.11.127.
[46] Zhang X, Zeng X, Yang M, Qi Y. Investigation of a branchlike MoO_3/polypyrrole hybrid with enhanced electrochemical performance used as an electrode in supercapacitors. ACS Appl Mater Interfaces 2014;6:1125–30. https://doi.org/10.1021/am404724u.
[47] Brezesinski T, Wang J, Tolbert SH, Dunn B. Ordered mesoporous α-MoO_3 with iso-oriented nanocrystalline walls for thin-film pseudocapacitors. Nat Mater 2010;9:146–51. https://doi.org/10.1038/nmat2612.
[48] Liu Y, Zhang B, Yang Y, Chang Z, Wen Z, Wu Y. Polypyrrole-coated α-MoO_3 nanobelts with good electrochemical performance as anode materials for aqueous supercapacitors. J Mater Chem A 2013;1:13582–7. https://doi.org/10.1039/c3ta12902k.
[49] Zhao G, Zhang N, Sun K. Porous MoO3 films with ultra-short relaxation time used for supercapacitors. Mater Res Bull 2013;48:1328–32. https://doi.org/10.1016/j.materresbull.2012.11.080.
[50] Li GR, Wang ZL, Zheng FL, Ou YN, Tong YX. ZnO@MoO_3 core/shell nanocables: facile electrochemical synthesis and enhanced supercapacitor performances. J Mater Chem 2011;21:4217–21. https://doi.org/10.1039/c0jm03500a.
[51] Xia X, Hao Q, Lei W, Wang W, Wang H, Wang X. Reduced-graphene oxide/molybdenum oxide/polyaniline ternary composite for high energy density supercapacitors: synthesis and properties. J Mater Chem 2012;22:8314–20. https://doi.org/10.1039/c2jm16216d.
[52] Khandare L, Late DJ. MoO_3-rGO nanocomposites for electrochemical energy storage. Appl Surf Sci 2017;418:2–8. https://doi.org/10.1016/j.apsusc.2016.11.199.
[53] Das AK, Karan SK, Khatua BB. High energy density ternary composite electrode material based on polyaniline (PANI), molybdenum trioxide (MoO_3) and graphene nanoplatelets (GNP) prepared by sono-chemical method and their synergistic contributions in superior supercapacitive p. Electrochim Acta 2015;180:1–15. https://doi.org/10.1016/j.electacta.2015.08.029.
[54] Yu F, Liu Y, Zhu Y, Dai F, Zhang L, Wen Z. Polypyrrole@MoO_3/reductive graphite oxide nanocomposites as anode material for aqueous supercapacitors with high performance. Mater Lett 2016;171:104–7. https://doi.org/10.1016/j.matlet.2016.01.028.
[55] Wu X, Wang Q, Zhang W, Wang Y, Chen W. Nanorod structure of Polypyrrole-covered MoO_3 for supercapacitors with excellent cycling stability. Mater Lett 2016;182:121–4. https://doi.org/10.1016/j.matlet.2016.05.176.
[56] Shakir I, Sarfraz M. Evaluation of electrochemical charge storage mechanism and structural changes in intertwined MoO_3-MWCNTs composites for supercapacitor applications. Electrochim Acta 2014;147:380–4. https://doi.org/10.1016/j.electacta.2014.09.073.
[57] Chen J, Han S, Zhao H, Bai J, Wang L, Sun G, et al. Robust wire-based supercapacitors based on hierarchical A-MoO_3 nanosheet arrays with well-aligned laminated structure. Chem Eng J 2017;320:34–42. https://doi.org/10.1016/j.cej.2017.03.041.
[58] Sangeetha DN, Krishna Bhat D, Selvakumar M. h-MoO_3/Activated carbon nanocomposites for electrochemical applications. Ionics (Kiel) 2018:1–24. https://doi.org/10.1007/s11581-018-2684-2.

Please cite this article as: Sangeetha DN et al., High power density and improved H_2 evolution reaction on MoO_3/Activated carbon composite, International Journal of Hydrogen Energy, https://doi.org/10.1016/j.ijhydene.2019.10.029